Desalination and Water Treatment
www.deswater.com

doi: 10.5004/dwt.2018.21929

108 (2018) 235–245
March

Estimation of nanofiltration membrane transport parameters for cobalt ions removal from aqueous solutions

Qusay F. Alsalhy[a,*], Ahmed A. Mohammed[b], Salwa H. Ahmed[c], Khalid T. Rashid[a], Mohammed A. AlSaadi[d,e]

[a]*Membrane Technology Research Unit, Chemical Engineering Department, University of Technology, Baghdad, Iraq, Tel. +964 7901730181; emails: qusay_alsalhy@yahoo.com, 80006@uotechnology.edu.iq (Q.F. Alsalhy), khalid.eng555@yahoo.com (K.T. Rashid)*
[b]*Environment Engineering Department, College of Engineering, University of Baghdad, Iraq, email: ahmed.abedm@yahoo.com*
[c]*Environment Engineering Department, College of Engineering, University of Tikrit, Iraq, email: env.salwa99@gmail.com*
[d]*Nanotechnology and Catalyst Research Center (NANOCAT), University of Malaya, Malaysia, email: mdsd68@gmail.com*
[e]*National Chair of Material Sciences and Metallurgy, University of Nizwa, Oman*

Received 14 June 2017; Accepted 20 January 2018

ABSTRACT

In the present work, three types of hollow fiber nanofiltration membranes (NF1, NF2 and NF3) were employed for the rejection and permeation flux of cobalt ions from aqueous wastewater. The operating variables—initial ion concentration (10–250 ppm), feed solution pH (5.5–6.5), pressure applied (1 bar) and feed flow rate (0.6 L/min)—were studied. It is observed that the obtained cobalt ion rejection values increase with the decrease in initial concentration and increase in pH at constant feed flow rate. The maximum observed rejection of the metal is found to be 77%, 50.2% and 46.8% and 38%, 30% and 29% for NF1, NF2 and NF3 for the initial feed concentration in the 10–250 ppm range, respectively. In addition, the flux decreases with the increase in both pH and initial concentration. Combined film theory–solution diffusion (CFSD), combined film theory–Spiegler-Kedem (CFSK) and combined film theory–finely porous (CFFP) membrane transport models were employed to estimate membrane transport parameters and mass transfer coefficient (k). Moreover, enrichment factor, concentration polarization modulus and Péclet number were estimated using various parameters. Analysis of the experimental data using CFSD, CFSK and CFFP models showed good agreement between theoretical and experimental results. Effective membrane thickness and active skin layer thickness were evaluated using CFFP model, indicating that the Péclet number is important for determining the mechanism of separation by diffusion.

Keywords: Nanofiltration; CFSK model; Heavy metals; Concentration polarization

1. Introduction

Rapid industrial growth, in developing countries in particular, has led to an increase in industrial waste discharge into the environment. These wastewaters comprise of dangerous toxic, such as heavy metals, and their discharge into the environment can pollute aquatic ecological environments and soil, thus threatening human health. Even an extremely low concentration of heavy metals in human body can result in abnormal physiological activities. Wastewaters of various industries such as paper, metal plating facilities and pesticide industries contain heavy metals. Unlike organic compounds, heavy metals do not decay and tend to accumulate in living organisms. Heavy metals in the wastewaters can also pollute rivers and underground water resources [1]. Cobalt is one of the heavy metals that may be present in the water. Co^{2+} is found naturally in the environment, for example, in rocks and

* Corresponding author.

soils. It is an important element for living beings because it is connected with the synthesis of vitamin B12. It is employed in the manufacture of alloys, paint driers, permanent magnets and industrial catalysts. Soil and sediment polluted with industrial waste can contain high levels of cobalt [2]. Several techniques have been utilized for wastewater treatment, including coagulation–flocculation, chemical precipitation, ion-exchange, evaporation, adsorption, biosorption and membrane filtration. Compared with other techniques, membrane technology has many advantages, such as (1) energy saving; (2) no phase change involved; (3) high separation efficiency; (4) easy to scale up and operate and (5) environmentally friendly [3].

The rejection of ionic solutes by nanofiltration can be controlled according to the following three steps: (1) The ions are transported through the polarization layer because of the concentration gradient attributable to the accumulation of ions near the membrane walls and the concentration of the bulk. (2) The solute equilibrium is established between the membrane external interface and the surrounding solution. (3) The dissolved substances (solutes) are transferred throughout the pores of the membrane itself. Nernst–Planck in their approach had adequate models for all the above mentioned steps together, considering all the governing electrical and dynamical effects transportation. However, these models were limited by the assumption of the existence of a perfect porous medium (i.e., an ideal porosity represented by a set of identical cylinders), which follows the classical continuous flow dynamics governing the equations. Although accurate description for the flow of permeability with the pressure can be achieved, the suitability of their model with practicality can be acquired by comparing the diameter of the pores from about 1 nm to that of the water molecules of about 0.3 nm. Recently, Yaroshchuk [4], Szymczyk and Fievet [5], Bandini and Vezzani [6], Bowen and Welfoot [7], and other authors had demonstrated that the dielectric effects along with steric and electrostatic effects can all be able to play an important role in the rejection of ionic species out of the nanofiltration membranes. However, if these effects are not fully understood nor have their interactions with electrical effects, their strength depends on the size of the pores in the same position that it may not be appropriate to consider the radius of a single pore and ignore the distribution of a pore size.

Owing to its unique rejection mechanisms steric effect and Donnan exclusion, nanofiltration (NF) is a widely used membrane filtration method. Compared with reverse osmosis, NF needs a lower pressure while giving a higher permeates flux without much compromise in rejection [8]. For this reason, the aim of the present study was to assess the performance of three types of NF membranes prepared for the purpose of heavy metal (i.e., cobalt Co^{2+} ions) removal under various conditions, such as feed solution pH and initial ion concentration. As available literature dedicated to the description of the concentration polarization and transport phenomena through the hollow fiber membranes is not described extensively, this work aims to address this gap. In addition, the estimation of membrane transport parameters and mass transfer coefficient by using the following theories has not been studied extensively to date: film theory, Combined film theory–Spiegler-Kedem (CFSK), Combined film theory–solution diffusion (CFSD), Combined film theory–finely porous (CFFP) models, and calculated concentration polarization model (CPM), enrichment factor (Eo) and Péclet number (Pe). Moreover, predictions provided by these models were compared with the experimental results.

2. Materials and methods

Simulated wastewater was prepared by adding the cobalt nitrate Co $(NO_3)_2.6H_2O$ to the distilled water. Stock solution (1,000 ppm) of Co^{2+} ions was prepared by dissolving the appropriate weight of cobalt nitrate in distilled water and was kept in polyethylene container at room temperature. The desired concentrations were prepared by diluting the stock solution in accurate proportions to different initial concentrations. Three different types of polyether sulfone (PES) NF membranes (PES type Radel, provided by Solvay Advanced Polymers, Belgium) were prepared by dry/wet phase inversion method under spinning parameters such as: extrusion pressure of 1.5 bar, bore fluid flow rate of 2.5 mL/min, 5 cm as air gap distance as well as pure water as internal and external coagulants, (denoted as NF1, NF2, and NF3) for the purpose of heavy metal removal. More details on the preparation of nanofiltration PES membrane can be found elsewhere [9,10]. The surface morphology and all the specifications of NF membranes are summarized in Table 1. pH values were measured using a calibrated pH meter (HQ411d, pH/mV, HACH Company, USA), whereas metal ion concentrations in simulated and treated solutions were tested using AAS-6200 atomic absorption flame emission spectrophotometer (Shimadzu Company, Japan). The device was calibrated regularly and the calibration curve was verified before each sample set.

The experiments of the nanofiltration performance using NF1, NF2 and NF3 hollow fibers were conducted by module cross-flow pattern filtration, as shown in Fig. 1. NF membrane experiments were carried out at a transmembrane pressure of 1 bar, solution temperature of 25°C ± 3°C, different initial metal concentrations (in the 10–250 ppm range) and 5.5–6.5 pH. It is obvious that the applied pressure for NF process is usually varied from 1 to 20–30 bar as it is reported in the literature, therefore, in this effort 1 bar was selected as applied pressure for the removal of heavy metals due to the low initial heavy metal concentrations. Permeate flux (J_V) (L/m^2 h) and heavy metal rejection (R%) were obtained from the following equations:

$$J_V = \frac{V}{t.A} \tag{1}$$

and

$$R(\%) = \left[1 - \frac{C_p}{C_b}\right] \times 100 \tag{2}$$

where V is the permeate volume (L), t is the collected permeate time (h), A is the membrane surface area (m^2) and C_p is the concentration of solute in permeate and C_b is an average bulk concentration of solute in the feed (C_f) and concentrate/retentate (C_r).

Table 1
Characteristics of the NF membranes

Type of membrane	NF1	NF2	NF3
Material	PES (29%)	PES (27%)	PES (27%)
Module	Hollow fiber	Hollow fiber	Hollow fiber
Length (cm)	22.2	22.7	23.1
Active area (m^2)	4.4×10^{-3}	5.7×10^{-3}	5.8×10^{-3}
Maximum operating temperature (°C)	45	45	45
Average pore size (nm)	52.04	58.11	47.75
Pore size distribution (nm)	25–100	35–130	20–115
Porosity (%)	52.5	67.6	58.1
Outer diameter (μm)	1,012	958.4	1,005
Inner diameter (μm)	620	576	603.6
Membrane thickness (μm)	196	191.2	200.7

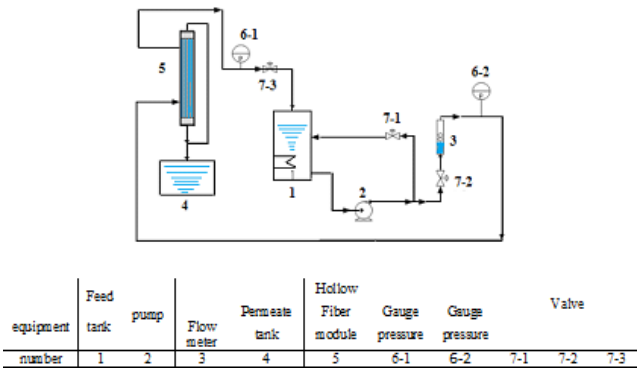

Fig. 1. Schematic diagram of the laboratory scale NF membrane system.

$$C_b = \frac{C_f + C_r}{2} \tag{3}$$

After each set of experiments for a given feed concentration, the setup was rinsed with distilled water for 60 min at 4 bar pressure to clean the NF membrane experimental system. This was followed by measurement of pure water permeation flux with distilled water to ensure that the initial membrane flux is restored. Moreover, pH value was adjusted using 1 M NaOH or 1 M HCl. By plotting the membrane flux (J_v) for a variation of applied pressure (ΔP), the membrane permeability (pure water permeability), L_p can be obtained from the slope of the straight line as follows:

$$L_p = \frac{J_v}{\Delta P} \tag{4}$$

3. Membrane transport models

3.1. Film theory

Accumulation of solute concentration at the membrane surface during separation process is termed as concentration polarization. The solute is transported into the boundary layer by convection and back to the bulk solution by diffusion [11,12].

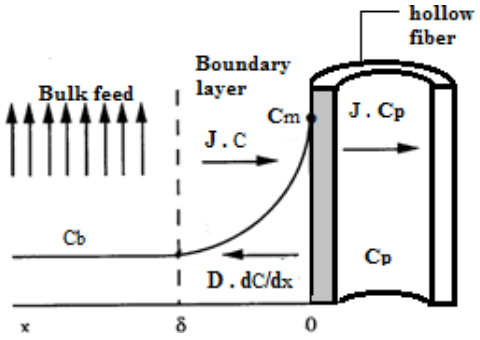

Fig. 2. Schematic of concentration polarization phenomenon in hollow fiber membrane.

It can be seen from Fig. 2 that the solute flux through the NF membranes decreases due to the concentration polarization phenomenon, where a gel layer forms on the surface of the membrane because of retained particles, resulting in an osmotic pressure increase. From simple mass balance, transport of solute at any point within the boundary layer can be explained by the relations given below [13]:

$$\left(C - C_p\right)J = D\frac{dc}{dx} \tag{5}$$

where D is the solute diffusivity, C is the solute concentration in the boundary layer, x is the distance from the membrane layer and C_p is the solute concentration on the permeate side. Eq. (5) can be integrated with respect to the following boundary conditions:

$C = C_m$ at $x = 0$, $\quad C = C_b$ at $x = \delta$

where C_m is the solute concentration at the membrane surface/water (solvent) interface, C_b is the solute in the bulk and δ is the edge of mass transfer boundary layer. This results in the following expressions:

$$\frac{C_m - C_p}{C_b - C_p} = \exp\left(\frac{J}{k}\right) \tag{6}$$

where k = mass transfer coefficient and is expressed as $k = D_{ab}/\delta$, D_{ab} = diffusivity of solute "a" in solvent "b" (cm^2/s).

The exemplary expressions of the observed R_o and true solute R rejections by a membrane are as follows [14]:

$$R_o = 1 - \frac{C_p}{C_b} \tag{7}$$

$$R = 1 - \frac{C_p}{C_m} \tag{8}$$

Using Eqs. (7) and (8), Eq. (6) can be rewritten in the following form [11]:

$$\ln\left(\frac{1-R_o}{R_o}\right) = \frac{1}{k}J + \ln\left(P_s\right) \tag{9}$$

where $P_s = \frac{1-R}{R}$.

By plotting $\ln(1-R_o/R_o)$ vs. J based on the experimental data, the mass transfer coefficient (k) and the overall permeability coefficient (P_s) can be estimated from the slope of the straight line and the intercept on the y-axis, respectively.

3.2. Combined film theory/solution diffusion model

This model describes the transport mechanism where the solvent and solute dissolves in the homogeneous, nonporous surface layer of the membrane. It is given by the equations as follows [15]:

$$J = L_p\left(\Delta P - \Delta\pi\right) \tag{10}$$

$$J_s = \left(\frac{D_{am}K}{\delta}\right)\left(C_m - C_p\right) \tag{11}$$

where L_p is the permeability parameter of the solvent and can be estimated from pure water permeability (PWP) measurements and $D_{am}K/\delta$ is regarded as a single parameter, namely the solute transport parameter.

$$\frac{R_o}{1-R_o} = \left[\frac{J}{D_{am}K/\delta}\right]\left[\exp\left(\frac{-J}{k}\right)\right] \tag{12}$$

Eq. (12) thus describes the CFSD model employed in the present study. By supplying R_o vs. J data, the parameter $D_{am}K/\delta$ and the mass transfer coefficient k can be estimated numerically.

3.3. Combined film theory/Spiegler-Kedem model

Kedem and Spiegler [16] reported that an irreversible thermodynamics (IT) model can be applied in the absence of electrostatic interaction between solute and membrane to describe the transport of single solute and solvent through an NF membrane. The process is described by a sum of convective (due to the difference of pressure) and diffusive (due to the concentration gradient at the membrane surface) fluxes. In IT, the membrane is treated as a black box. Thus, physicochemical membrane properties and solution system are treated as model parameters. The working equations of the nonlinear Spiegler-Kedem model [16,12] are:

$$J = -L_p(\Delta p - \sigma\Delta\pi) \tag{13}$$

$$J_s = -P_M\Delta C_s + (1-\sigma)C_sJ \tag{14}$$

Assuming constant fluxes and constant coefficients σ and P_M, Eq. (14) is integrated through the membrane thickness. This leads to the well-known Spiegler-Kedem equation, which relates the solute retention with the solvent volumetric flux and the solute permeability:

$$R = \frac{\sigma(1-F)}{1-\sigma F} \tag{15}$$

where

$$F = \exp[-Ja2] \tag{16}$$

with

$$a2 = \frac{1-\sigma}{P_M} \tag{17}$$

where σ is reflection coefficient which assimilates the rejection capability of a membrane, that is, $\sigma = 0$ indicates no rejection and $\sigma = 1$ denotes 100% rejection; P_M is salt permeability (L/m^2 h) and L_p is the hydraulic permeability coefficient of the membrane. F = flow parameter. Eq. (15) can be rearranged to give:

$$\frac{R}{1-R} = a1(1-F) \tag{18}$$

where

$$a1 = \frac{\sigma}{1-\sigma} \tag{19}$$

Now, substituting Eq. (18) into Eq. (9) results in the following equation:

$$\frac{R_o}{1-R_o} = a1\left[1-\exp(-Ja2)\right]\left[\exp\left(\frac{-J}{k}\right)\right] \tag{20}$$

Eq. (20) represents CFSK model. The membrane σ, P_M and mass transfer coefficient k can be estimated by using a nonlinear parameter estimation method (SPSS version 22), where R_o vs. J at different conditions serve as model inputs [17].

3.4. Combined film theory/finely porous model

The CFFP model incorporates the friction effect between solid molecules and membrane pore wall. A factor b is

introduced to take into account the friction impact. The working equation is given below [18]:

$$\frac{1}{1-R}=\left(\frac{b_f\varepsilon}{k}\right)+\left(\frac{k-b_f\varepsilon}{k}\right)\exp\left(-J\frac{\tau\varepsilon}{\varepsilon b_f D_{ab}}\right) \tag{21}$$

where b_f is factor measure of friction between the solute molecules and the membrane pore wall, where calculated from $b_f = 1+ f_{sm}/f_{sw}$; where f_{sm} = friction coefficient between solute and membrane, while f_{sw} = friction coefficient between solute and solvent (water).

Replacement of Eq. (21) into Eq. (9) results in the following equation:

$$\frac{R_o}{1-R_o}=\left(\frac{b_f\varepsilon}{k}-1\right)\left[1-\exp\left(-J\frac{\tau\delta}{\varepsilon b_f D_{ab}}\right)\right]\exp\left(-\frac{J}{k}\right) \tag{22}$$

where

$$b1=\left(\frac{b_f\varepsilon}{k}-1\right) \tag{23}$$

$$b2=\frac{\tau\delta}{\varepsilon b_f D_{ab}} \tag{24}$$

Eq. (22) is the CFFP model. The membrane parameters and k can be estimated via a nonlinear parameter estimation method (SPSS version 22) by supplying the data for R_o vs. J taken at various conditions for each set.

3.5. Concentration polarization model and enrichment factor

Concentration polarization is usually characterized via film theory model, where it is described by the thickness of the boundary layer across which the counter diffusion occurs. Here, the concentration terms of Eq. (6) are replaced by an enrichment factor E, known as C_p/C_b. Moreover, as Eo represents C_p/C_m, concentration polarization can be expressed by Péclet number (Pe), therefore, Eq. (6) can be written as follows [19]:

$$\frac{1/\mathrm{Eo}-1}{1/E-1}=\exp(\mathrm{Pe}) \tag{25}$$

where Pe = J/k.

Any variation in solute concentration (increase or decrease) at the membrane surface compared with the concentration of bulk solution determines the range of concentration polarization. The ratio of the two concentrations, C_m/C_b, represents the CPM and is a good indication of the range of concentration polarization. When CPM ≤ 1, no CP takes place. On the other hand, the model neutralized farther from > 1, the impact of CP on membrane selectivity and flux becomes important. From the definition of Eo and E, the CPM equivalent of Eo and E and from Eqs. (6) and (10) can be written as [19,17]:

$$\frac{E}{\mathrm{Eo}}=\frac{C_m}{C_b}=\frac{\exp(\mathrm{Pe})}{1+\mathrm{Eo}[\exp(\mathrm{Pe})-1]} \tag{26}$$

Also, C_m can be found from Eqs. (26) and (27) below [20]:

$$\frac{C_m}{C_b}=(1-R_o)+R_o\exp(J/k) \tag{27}$$

where $R_o = 1 - C_p/C_m$

According to the enrichment code Eo of the hollow fiber, the CP modulus could be higher or lower than one. Eq. (26) shows the parameters that estimate the value of CP, it mean the thickness of the boundary layer δ, the hollow fiber enrichment Eo, the volumetric flow rate across the hollow fiber J, and solute diffusion coefficient within the boundary layer fluid D. The most important parameter that affects CP is δ. When δ reduces, Eq. (26) presents that the CP modulus be exponentially lower. Therefore, the important method for decreasing the CP is to decrease δ by accelerating the turbulent around the hollow fiber surface [21]. The real enrichment of the hollow fiber Eo, also affects CP. For example, Eo = 1, if the fiber membrane is totally unselective. The concentrations of the species permeating within the fiber membrane do not alter; therefore, in the boundary layer the concentration difference is not created. Moreover, when the difference in permeability of the species increases, the real enrichment Eo of the fiber enhances, and the concentration difference that is created in the boundary layer becomes higher. Also, another significant characteristic of Eq. (26) is that Eo generated by the fiber, not the real selectivity α, determines the separation performance of the fiber and the CP modulus. Eq. (26) shows that CP increases exponentially with increase of the total volumetric flow rate J across the hollow fiber.

3.6. Comparison of model predictions and the experimental results (S^2)

Validity of the models examined in the present study and the fitting type employed were ascertained by determining the nonlinear parameters via the relationship below [20]:

$$S^2=\sum\left(R_{\mathrm{exp}}-R_{\mathrm{th}}\right)^2/R_{\mathrm{th}} \tag{28}$$

where R_{exp} and R_{th} are the experimental rejection and theoretical rejection calculated in accordance with the models, respectively. If $R_{exp} \le R_{th}$ then S^2 will be a small number, while $R_{exp} > R_{th}$ would lead to large S^2.

3.7. Determining Péclet number (Pe)

The Pe (a dimensionless number) is an important factor in the study of transport phenomena in fluid flows. It corresponds to the ratio between the convective transport J of a physical quantity and the flow and diffusive transport k (= D_{ab}/δ) of the same quantity driven by an appropriate gradient. The Péclet number is defined as:

$$\mathrm{Pe} = \frac{\text{advective transport rate}}{\text{diffusive transport rate}}$$

$$\mathrm{Pe} = \frac{J}{k} \tag{29}$$

where k denotes the mass transfer coefficient from the CFSK model [17].

4. Results and discussion

4.1. Permeability of NF membranes

PWP measurements as a function of transmembrane pressure (TMP) for three types of nanofiltration membranes were carried out by using Eq. (1), as shown in Fig. 3. It can be seen that PWP increased linearly when TMP increased from 1 to 4 bar, indicating that the membrane performance was not significantly affected by fouling. The membrane permeability for NF2, NF3 and NF1 was 37.9 > 16.6 > 16.4 (L/m² h bar), at 1 bar transmembrane pressure, respectively. This behavior is due to the higher NF2 porosity relative to other membranes, as shown in Table 1. This behavior is similar to that found by Semiao and Schafer [22], who reported the permeability of about 18 L/m² h bar. The concentration polarization and fouling of the membranes are evaluated according to the permeability of water solution as reported by Murthy and Chaudhari [17], and accordingly the cleaning procedure is evaluated.

4.2. Effects of the feed solution pH

Figs. 4 and 5 show the effect of the pH of the feed solution on the permeate flux and rejection of cobalt ions using three types of NF membranes for 100 ppm initial Co^{2+} ion concentrations at different times. Generally, it can be noticed that the permeate flux of all solutions decreases with the increase in feed solution pH from 5.5 to 6.5. Permeate flux decreased from 7.4 to 6.3 (L/m² h), 23.3 to 18.2 (L/m² h) and 13.8 to 9.5 (L/m² h) as the feed solution pH increased from 5.5 to 6.5 using NF1, NF2 and NF3 for Co^{2+} ions, respectively. Moreover, the cobalt rejection increased with the increase in the pH value. The rejection increased from 19% to 28% using NF1 with an increase in pH from 5.5 to 6.5. The rejection of Co^{2+} ions increased from 28% to 44.5% with the increase in pH from 5.5 to 5.7, while the rejection of Co^{2+} ions decreased to 31% at pH value 6 using NF2. Moreover, using NF3 membrane, Co^{2+} ion rejection increased from 23% to 35% with the increase in pH from 5.5 to 6, while the rejection of Co^{2+} ions decreased significantly to 33% at pH 6.5. This phenomenon is mainly attributed to the charge of the membrane surface, as increasing pH from 5.5 to 6.5 results in a more negative membrane charge due to the increase in OH^-. Therefore, adsorption of heavy metal ions occurs at the surface of the hollow fiber membrane because of the electrostatic attraction, which in turn leads to a decrease in membrane pore size, decreasing the permeation flux and increasing rejection. Moreover, membrane charge can also vary significantly due to equilibrium of the surface groups of the membrane. Childress and Elimelech [23] suggested mechanisms to explicate change in flux as a result of changing the pores size with pH, which are due to (i) expansion or contraction associated with a network of polymer membrane, (ii) decreased electro-viscous effect and (iii) net driving force being higher than the osmotic pressure on the membrane surface. Another explanation is due to shrinkage of the membrane

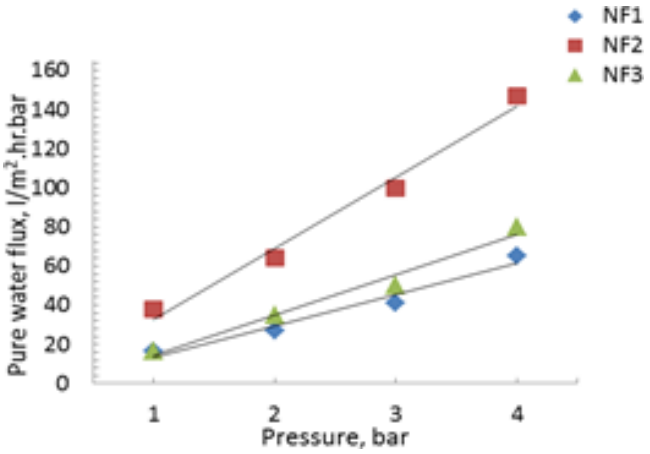

Fig. 3. Pure water permeability as a function of TMP for NF membrane.

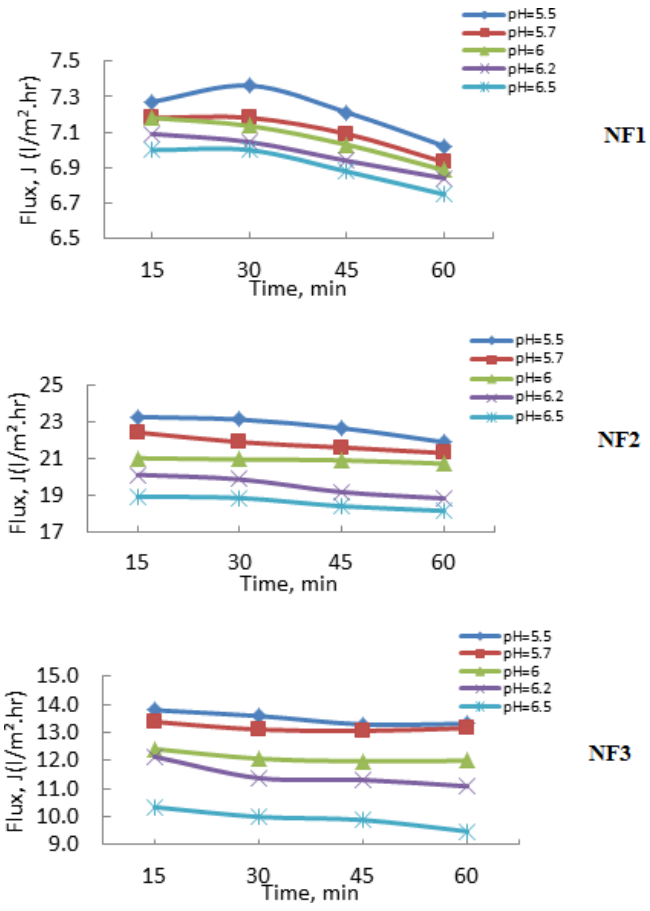

Fig. 4. Effect of feed pH solution on permeate flux of NF membranes at different times (pH 5.5–6.5; time 15–60 min; initial concentration of Co ion 100 ppm).

layer as a result of differences in the hydration of membrane ionized groups [24]. Moreover, Wang et al. [25] and Tanninen et al. [26] posited that this change is due to concentration polarization and membrane fouling.

4.3. Effect of initial ion concentrations

Figs. 6 and 7 show the effects of the initial concentration of Co^{2+} ions on the permeate flux and rejection for the three types of NF membranes (at the best initial pH value obtained from the study of the effect of pH) at different times. It can be observed that the permeate flux significantly decreased, that is, from 7.6 to 5 (L/m^2 h), 23.9 to 20.2 (L/m^2 h) and 14.5 to 9.6 (L/m^2 h), as the initial Co^{2+} ion concentration increased from 10 to 250 ppm for NF1, NF2 and NF3, respectively. In addition, Co rejection decreases with the increase in the initial ion concentration, that is, from 10 to 250 ppm, from 77% to 33%, 49.2% to 28.2% and 46.8% to 22% when NF1, NF2 and NF3 are used, respectively. The reason of the flux decline is caused by electrostatic interactions that are progressively screened due to the increase in ionic strength as reported by Deon et al. [27].

4.4. Estimation of membrane transport parameters

Based on the Levenberg–Marquardt method [28] the experimental data were analyzed using the SPSS version 22 nonlinear parameter estimation program, where observed rejection (R_o) and permeate flux (J) were calculated at different parameter conditions (feed pH, NF membrane type and initial ion concentration) for each data set. The parameters estimated by applying different models expressed by Eqs. (12), (20) and (22) were employed to calculate the NF membrane transport parameters and mass transfer coefficients according to the respective relations. To obtain R_o of the NF membrane for different J values, these parameters were subsequently used with regard to the individual model, as depicted in Table 2. Comparisons between the experimental and theoretical results are shown in Fig. 8, and can also be discerned through the values of nonlinear parameters S^2 presented in Table 2. Where, the experimental results are substituted by the theoretical equations and the values of the parameters are calculated. Then, these parameters were substituted again in the equations in order to find the second values of efficiency and J by applying a statistical program using trial and error method.

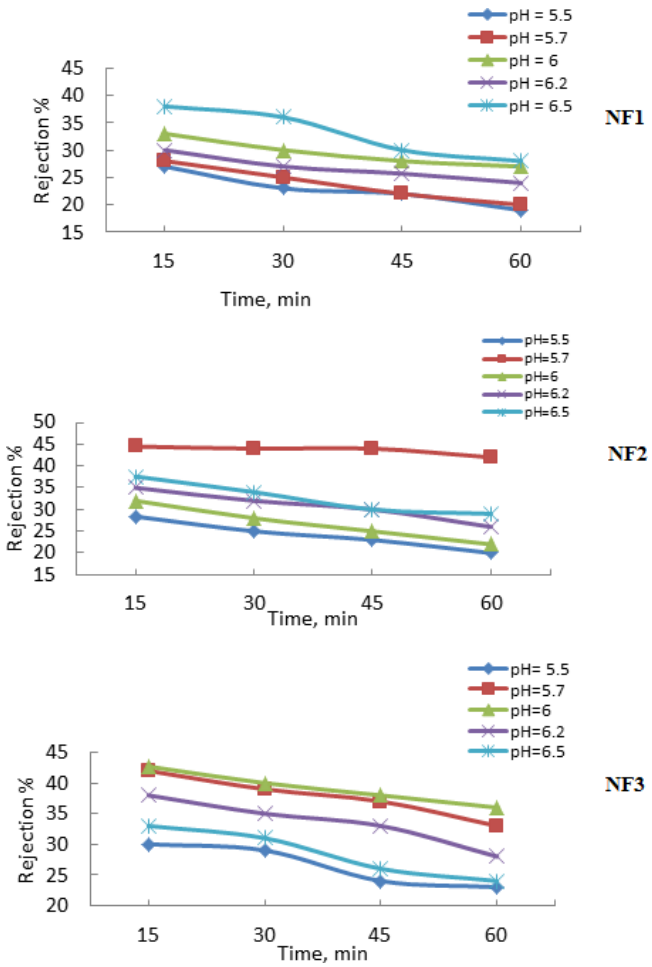

Fig. 5. Effect of feed pH solution on rejection of NF membranes at different times (pH 5.5–6.5; time 15–60 min; initial concentration of Co ion 100 ppm).

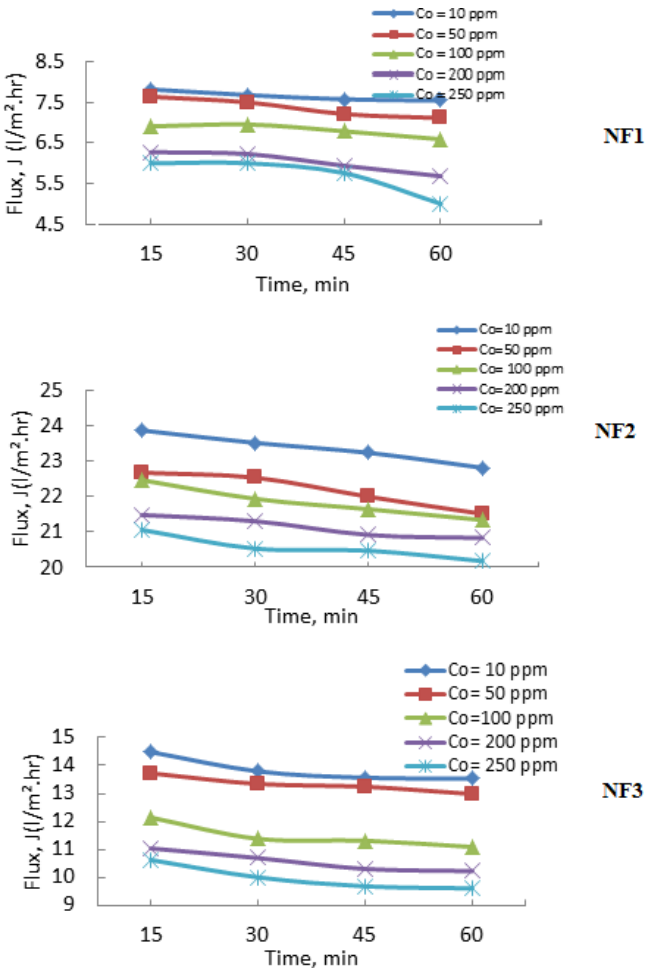

Fig. 6. Effect of initial metal ions concentration on flux of NF membranes at different times (time 15–60 min; initial concentration of Co ion 10–250 ppm).

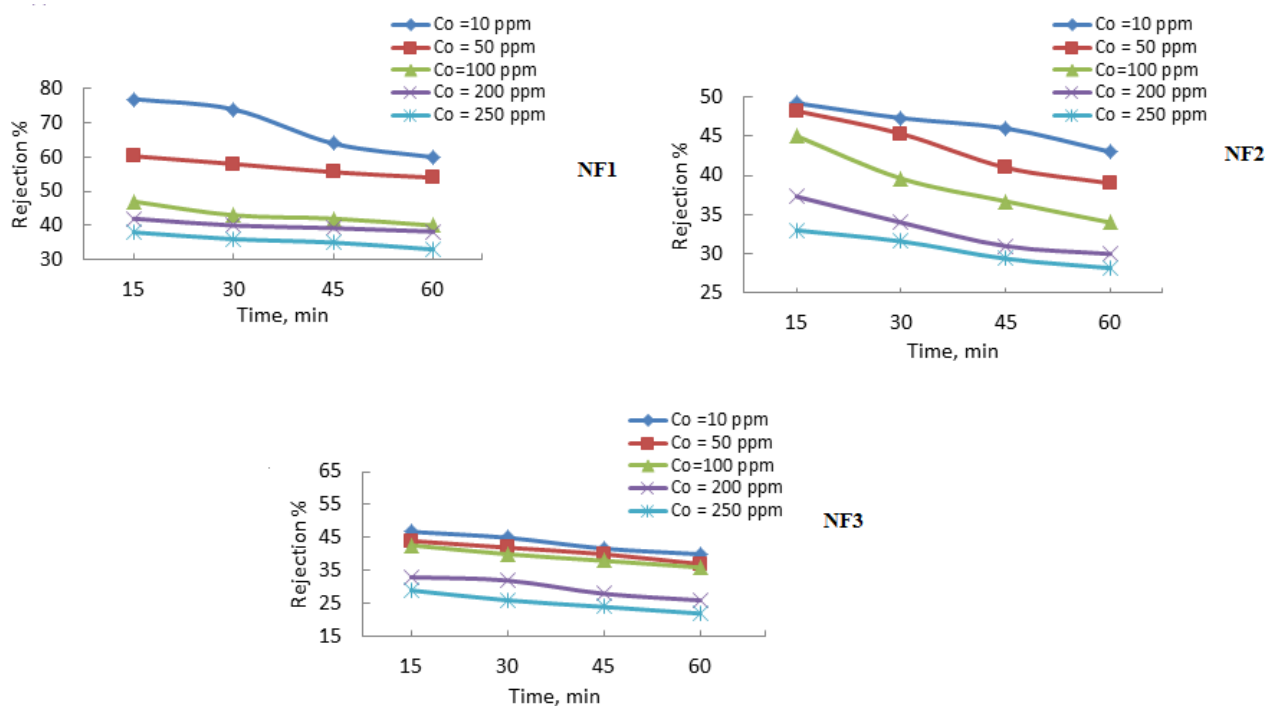

Fig. 7. Effect of initial metal ions concentration on rejection of NF membranes at different times (time 15–60 min; initial concentration of Co ion 10–250 ppm).

Table 2
Parameter estimated for various modules by a nonlinear estimated program

Type of membrane	No. of set	pH	Feed concentration (ppm)	CFSD model		CFSK model				CFFP model	
				$D_{am}K^a/\delta \times 10^4$ (cm/s)	$k^b \times 10^3$ (cm/s)	σ	$P_M \times 10^5$ (cm/s)	$k^b \times 10^3$ (cm/s)	S^2	ε/k^b	$\varepsilon D_{ab}/\tau\delta \times 10^4$
NF1	1	5.5	10	2.45	4.48	0.9121	5.51	20.31	0.098	7.88	9.51
	2	5.5	50	2.34	4.44	0.9098	5.88	20.11	0.104	7.96	9.57
	3	5.5	100	2.38	4.45	0.9011	6.23	19.65	0.124	8.14	9.88
	4	5.5	200	2.41	4.37	0.8971	7.19	19.55	0.157	8.18	9.92
	5	5.5	250	2.35	3.98	0.8945	8.55	19.02	0.072	8.41	10.11
NF2	6	5.7	10	2.55	4.38	0.9101	5.59	21.31	0.06	7.51	9.61
	7	5.7	50	2.43	4.32	0.9078	5.98	21.11	0.073	7.58	9.81
	8	5.7	100	2.31	4.35	0.8911	6.13	19.94	0.06	8.02	10.11
	9	5.7	200	2.46	3.19	0.8881	7.09	19.65	0.134	8.14	9.98
	10	5.7	250	2.25	3.77	0.8767	7.55	19.32	0.069	8.28	11.12
NF3	11	6	10	2.51	4.76	0.9201	5.88	21.11	0.071	7.58	9.67
	12	6	50	2.53	4.56	0.9178	6.88	20.81	0.074	7.69	9.81
	13	6	100	2.66	4.54	0.9011	7.13	20.14	0.121	7.94	9.98
	14	6	200	2.58	4.12	0.8981	7.89	19.95	0.238	8.02	10.12
	15	6	250	2.67	3.97	0.8907	7.98	19.12	0.272	8.37	10.41

[a]Solute partition coefficient.
[b]Value of mass transfer coefficient of CFSD, CFSK and CFFP model.

Both outputs confirm that all the results are equally fitted. Moreover, the model-predicted ion concentrations for specific rejection values are in good agreement with the experimental results.

The CFSK model shows a high degree of accuracy when applied to the experimental rejection data for all of the initial metal concentrations and NF membrane types. In sum, very high reflection coefficients (σ) and very low values of permeability solute (P_s) were obtained by fitting the CFSK model to the experimental data. As these parameters are based on initial metal concentrations, P_s increases as the initial metal concentration increases due to the high solute amount

crossing through the membrane. On the other hand, a gradual decrease in the solute rejection reduction is observed with changes in σ. The same result was obtained by Al-Zoubi [29].

These results explicate the transport mechanism of solutes in these processes by same remarks. At low pressure, a high transport diffusive of solute is dependable for low rejection. While at high pressure, convective solute transport is more important, this effect was not observed in our experimental results because the rejection was high even at low pressures. Thus, convective transport seems to be dominant in the rejection processes under study. Moreover, σ is a measure of the hinder of the convective solute transport within the NF membrane [30]. Therefore, the Spiegler-Kedem parameter values ensure that the previous results reflect the membrane structure. In 2013, Ballet et al. [24] examined the impact of Co ion characteristics on the solute rejection, reporting that the reflection coefficient (σ) for each solute increases with the increase in Co ion valence, while P_s decreases. Similar results were obtained by Wang et al. [31]. For the CFFP model, the effective membrane thickness (τδ/ε) can be determined from the average value of parameter b2, and was previously calculated as 255 μm [32]. If the values of membrane void fraction (ε) and tortuosity (τ) are assumed to be 0.16 and 3, respectively [33], thickness of the boundary layer (δ) will be 14, which is a reasonable value with regard to the data submitted by the supplier.

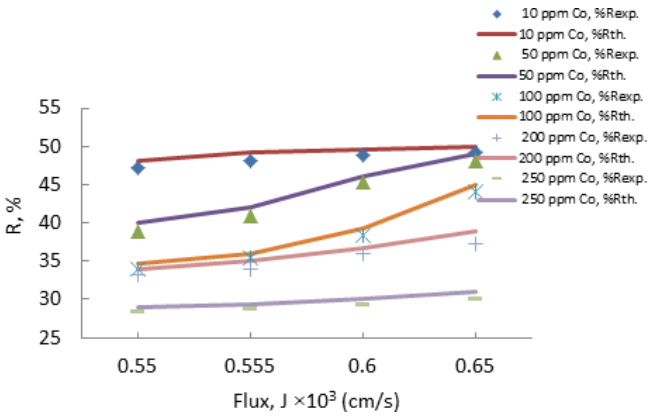

Fig. 8. Results of CFSK model for data set of NF2 membrane for Co $(NO_3)_2$ at different times.

4.5. Estimation of concentration polarization model and enrichment factors Eo and E

To calculate the true rejection by using membrane transport model which depends on concentration polarization, Eq. (25) was applied, as it includes the factors that impact on concentration polarization, namely the permeate volume flux, diffusion coefficient of the solute in the thickness of the boundary layer (δ), and the membrane enrichment factor (which depends on the C_p/C_b ratio). In Table 3, the enrichment factors Eo and *E* for the three types of NF membranes and solute (Co^{2+}) ions are given. It can be seen that the concentration of solute at the membrane surface is 1.0032 to 1.0082, 1.0097 to 1.0149 and 1.004 to 1.0083 times greater than that in the absence of concentration polarization of NF1, NF2 and NF3, respectively. With respect to reverse osmosis, the concentration polarization models are usually about 1.1 and 1.5 [24], while Eo ranged from 0.23 to 0.64, from 0.508 to 0.67 and from 0.55 to 0.71, for NF1, NF2 and NF3, respectively. Regarding to reverse osmosis, the enrichment factors are usually about 0.01 [24], due to the membrane solute rejection capability of about 100%. Similar results were obtained by Murthy and Chaudhari [17].

The comparison between concentration polarization and Péclet number for NF1, NF2 and NF3 membrane at different Co^{2+} ion concentrations is shown in Table 3. When the

Table 3
Summary of CPM, enrichment factors (Eo and *E*) and Péclet number

Type of membrane	No. of set	pH	Feed concentration (ppm)	Enrichment factors		CPM C_m/C_b	$k^a \times 10^3$ (cm/s)	Permeate flux (×10³) (cm/s)	Péclet number (J/k^a)
				E	Eo				
NF1	1	5.5	10	0.2300	0.2281	1.0082	20.31	0.217	0.0107
	2	5.5	50	0.4000	0.3975	1.0062	20.11	0.208	0.0104
	3	5.5	100	0.5800	0.5776	1.0042	19.65	0.194	0.0099
	4	5.5	200	0.6000	0.5979	1.0035	19.55	0.172	0.0088
	5	5.5	250	0.6400	0.6380	1.0032	19.02	0.167	0.0088
NF2	6	5.7	10	0.508	0.5006	1.0149	21.31	0.6444	0.0302
	7	5.7	50	0.518	0.5109	1.0139	21.11	0.6111	0.0289
	8	5.7	100	0.55	0.5428	1.0133	19.94	0.5917	0.0297
	9	5.7	200	0.627	0.6202	1.0109	19.65	0.5778	0.0294
	10	5.7	250	0.67	0.6636	1.0097	19.32	0.5694	0.0295
NF3	11	6.0	10	0.55	0.5455	1.0083	21.11	0.3889	0.0184
	12	6.0	50	0.58	0.5757	1.0074	20.81	0.3667	0.0176
	13	6.0	100	0.573	0.5690	1.0071	20.14	0.3361	0.0167
	14	6.0	200	0.67	0.6669	1.0047	19.95	0.2833	0.0142
	15	6.0	250	0.71	0.7071	1.0040	19.12	0.2667	0.0139

[a]Value of mass transfer coefficient of CFSK model and CFFP model.

Péclet number is large ($J >> k$), the convective flux through the membrane cannot be easily stabilized by diffusion in the boundary layer, and concentration polarization models will be large. On the other hand, when the Péclet number is small ($J << k$), the convective flux through the membrane can be easily stabilized by diffusion in the boundary layer, and concentration polarization models are close to unity [15]. The Péclet number values ranged from 0.0088 to 0.0107, from 0.0303 to 0.0312 and from 0.0154 to 0.0191 for NF1, NF2 and NF3, respectively. Therefore, the Péclet number is an important factor for determining the mechanism of separation by diffusion. It is also worth noting that similar results were reported by Soltanieh and Gill [33].

5. Conclusions

In the present study, three NF membranes were used for separation of cobalt from simulated wastewater. NF membrane performance was interpreted in terms of permeate volume flux and ion rejection. It was observed that the flux decreases with the increase of feed solution pH, while the rejection of solute increases with the increase of pH from 5.5 to 6.5. Permeate flux and rejection of NF membranes decrease with the increase in initial ion concentration at constant feed flow rate, resulting from the concentration polarization and fouling. In addition, permeate flux and rejection depend strongly on the ion type, diffusion coefficient, charge valence and hydration energy. The maximum rejection of solute was 77%, 50.2% and 46.8% of Co^{2+} for NF1, NF2 and NF3 at 10 ppm initial ion concentration, respectively. Analysis of the experimental data using CFSD, CFSK and CFFP models showed good agreement between theoretical and experimental results. Moreover, the active skin layer thickness and the effective membrane thickness were predicted by the CFFP model. Finally, Péclet number was found to be an important factor for determining the mechanism of separation by diffusion.

Symbols

A	—	Membrane surface area, m^2
b_f	—	Factor measure of friction between the solute molecules and the membrane pore wall, where calculated from $b_f = 1 + f_{sm}/f_{sw}$
C	—	Solute concentration in the boundary layer, g/m^3
C_b	—	Average bulk concentration, g/m^3
C_f	—	Concentration of solute in the feed, g/m^3
CFFP	—	Combined film theory/finely porous model
CFSD	—	Combined film theory/solution diffusion model
CFSK	—	Combined film theory/Spiegler-Kedem model
C_m	—	Solute concentration at the membrane surface/water (solvent) interface, g/m^3
CP	—	Concentration polarization
C_p	—	Concentration of solute in permeate, g/m^3
CPM	—	Concentration polarization model
C_r	—	Concentration of solute in retentate, g/m^3
D_{am} K/δ	—	Solute transport parameter, cm/s
D	—	Diffusion coefficient, cm^2/s
D_{ab}	—	Diffusivity of solute "a" in solvent "b", cm^2/s
D_{am}	—	Diffusivity of salt "a" on surface membrane, cm^2/s
Eo	—	Enrichment factor known as C_p/C_m
F	—	Flow parameter defined in Eq. (16)
f_{sm}	—	Friction coefficient between solute and membrane
f_{sw}	—	Friction coefficient between solute and solvent (water).
J_S	—	Solute flux through membrane, m^3/m^2s
J_v	—	Convective + diffusive mass transfer rate, $m^3/m^2\,s$
K	—	Solute partition coefficient
k	—	Mass transfer coefficient and is expressed as $k = D_{ab}/\delta$
Pe	—	Péclet number (a dimensionless number)
PES	—	Polyether sulfone
P_M	—	Salt permeability, L/m^2 h
P_s	—	Overall permeability coefficient
PWP	—	Pure water permeability
R	—	True solute rejections
R_{exp}	—	Experimental rejection
R_o	—	Observed rejection
R_{th}	—	Theoretical rejection
t	—	Collected permeate time, h
TMP	—	Transmembrane pressure, bar
V	—	Permeate volume, L
x	—	Distance from the membrane layer, m

Greek letters

ε	—	Membrane void fraction
τ	—	Tortuosity
δ	—	Layer thickness; thickness of the boundary layer, m
$\frac{\tau\delta}{\varepsilon}$	—	Effective membrane thickness
ΔP	—	Transmembrane pressure, bar
$\Delta\pi$	—	Osmotic pressure difference, bar

References

[1] A. Maher, M. Sadeghi, A. Moheb, Heavy metal elimination from drinking water using nanofiltration membrane technology and process optimization using response surface methodology, Desalination, 352 (2014) 166–173.
[2] S.K. Sharma, Heavy Metals in Water: Presence, Removal and Safety, Published by the Royal Society of Chemistry, 2015, Available at: www.rsc.org.
[3] W. Zhu, S. Sun, J. Gao, F. Fu, T. Chung, Dual-layer polybenzimidazole/polyethersulfone (PBI/PES) nanofiltration (NF) hollow fiber membranes for heavy metals removal from wastewater, J. Membr. Sci., 456 (2014) 117–127.
[4] A.E. Yaroshchuk, Non-steric mechanisms of nanofiltration: superposition of Donnan and dielectric exclusion, Sep. Purif. Technol., 22 (2001) 143.
[5] A. Szymczyk, P. Fievet, Investigating transport properties of nanofiltration membranes by means of a steric, electric and dielectric exclusion model, J. Membr. Sci., 252 (2005) 77–88.
[6] S. Bandini, D. Vezzani, Nanofiltration modeling: the role of dielectric exclusion in membrane characterization, Chem. Eng. Sci., 58 (2003) 3303.
[7] W.R. Bowen, J.S. Welfoot, Modelling the performance of membrane nanofiltration-critical assessment and model development, Chem. Eng. Sci., 57 (2002) 1121.

[8] H.Y. Shim, K.S. Lee, D.S. Lee, D.S. Jeon, M.S. Park, J.S. Shin, Y.K. Lee, J.W. Goo, S.B. Kim, D.Y. Chung, Application of electrocoagulation and electrolysis on the precipitation of heavy metals and particulate solids in wash water from the soil washing, J. Agric. Chem. Environ., 3 (2014) 130–138.
[9] Q. Alsalhy, S. Algebory, G.M. Alwan, A. Figoli, S. Simone, E. Drioli, Hollow fiber ultrafiltration membranes from poly(vinyl chloride): preparation, morphologies and properties, Sep. Sci. Technol., 46 (2011) 1–12.
[10] Q.F. Alsalhy, H.A. Salih, R.H. Melkon, Y.M. Mahdi, N.A. Abdul Karim, Effect of the preparation conditions on the morphology and performance of poly(imide) hollow fiber membranes, J. Appl. Polym. Sci., 131 (2014) 40428.
[11] R.A. Hajarat, The Use of Nanofiltration Membrane in Desalinating Brackish Water, PhD Thesis, School of Chemical Engineering and Analytical Science, University of Manchester, 2010.
[12] C.V. Gherasim, J. Cuhorka, P. Mikulášek, Analysis of lead (II) retention from single salt and binary aqueous solutions by a polyamide nanofiltration membrane: experimental results and Modeling, J. Membr. Sci., 436 (2013) 132–144.
[13] R.B. Bird, W.E. Stewart, E.N. Lightfoot, Transport Phenomena, 2nd ed., John Wiley & Sons, Inc., New York, 2002.
[14] S. Lee, G. Amy, J. Cho, Applicability of Sherwood correlations for natural organic matter (NOM) transport in nanofiltration (NF) membranes, J. Membr. Sci., 240 (2004) 49–65.
[15] K.R. Desai, Z.V.P. Murthy, Removal of Ag(I) and Cr (VI) by complexation-ultrafiltration and characterization of the membrane by CFSK model, Sep. Sci. Technol., 49 (2014) 2620–2629.
[16] O. Kedem, K. Spiegler, Thermodynamics of hyper-filtration (reverse osmosis): criteria for efficient membrane, Desalination, 1 (1966) 311–326.
[17] Z.V.P. Murthy, L.B. Chaudhari, Application of nanofiltration for the rejection of nickel ions from aqueous solutions and estimation of membrane transport parameters, J. Hazard. Mater., 160 (2008) 70–77.
[18] S.Y. Vaidya, A.V. Simaria, Z.V.P. Murthy, Reverse osmosis transport models evaluation: a new approach, Ind. J. Chem. Technol., 8 (2001) 335–343.
[19] R. Baker, Membrane Technology and Applications, 2nd ed., Wiley, 2004.
[20] K.Y. Foo, Hameed, Insight into the modeling of adsorption isotherm systems, Chem. Eng. J., 156 (2010) 2–10.
[21] G. Belfort, R.H. Davis, A.L. Zydney, The behavior of suspensions and macromolecular solutions in cross flow microfiltration, J. Membr. Sci., 96 (1994) 1–58.
[22] A.J.C. Semiao, A.I. Schafer, Estrogenic micro-pollutant adsorption dynamics onto nanofiltration membranes, J. Membr. Sci., 381 (2011) 132–141.
[23] A.E. Childress, M. Elimelech, Relating nanofiltration membrane performance to membrane charge (electrokinetic) characteristics, Environ. Sci. Technol., 34 (2000) 3710–3716.
[24] G.T. Ballet, L. Gzara, A. Hafiane, M. Dhahbi, Transport coefficients and cadmium salt rejection in nanofiltration membrane, Desalination, 167 (2004) 369–376.
[25] Z. Wang, G. Liu, Z. Fan, X. Yang, J. Wang, S. Wang, Experimental study on treatment of electroplating wastewater by nanofiltration, J. Membr. Sci., 305 (2007) 185–195.
[26] J. Tanninen, S. Platt, A. Weis, M. Nystrom, Long-term acid resistance and selectivity of NF membranes in very acidic conditions, J. Membr. Sci., 240 (2004) 11–18.
[27] S. Deon, P. Dutournie, P. Bourseau, Transfer of monovalent salts through nanofiltration membranes: a model combining transport through pores and the polarization layer, Ind. Eng. Chem. Res., 46 (2007) 6752–6761.
[28] M.S. Bazaraa, H.D. Sherali, C.M. Shetty, Nonlinear Programming Theory and Algorithms, 2nd ed., Wiley, New York, 1993.
[29] H. Al-Zoubi, Development of novel approach to the prediction of nanofiltration membrane performance using advanced atomic force microscopy, Thesis, University of Nottingham, 2006.
[30] J. Schaep, B. Van der Bruggen, S. Uytterhoeven, R. Croux, C. Vandecasteele, D. Wilms, E. Van Houtte, F. Vanlerberghe, Removal of hardness from groundwater by nanofiltration, Desalination, 119 (1998) 295–302.
[31] X. Wang, T. Tsuru, N. Shin-Ichi, S. Kimura, Electrolyte transport through nanofiltration membrane by the space-charge model and the comparison with Teorell-Meyer-Sievers model, J. Membr. Sci., 103 (1995) 117–133.
[32] Z.V.P. Murthy, L.B. Chaudhari, Separation of binary heavy metals from aqueous solutions by nanofiltration and characterization of the membrane using Spiegler–Kedem model, Chem. Eng. J., 150 (2009) 181–187.
[33] M. Soltanieh, W.N. Gill, Review of reverse osmosis membranes and transport models, Chem. Eng. Commun., 12 (1981) 279–363.